J Mater Sci (2011) 46:3716–3724
DOI 10.1007/s10853-011-5273-6

Controlled mechanochemically assisted synthesis of ZnO nanopowders in the presence of oxalic acid

A. Stanković · Lj. Veselinović · S. D. Škapin · S. Marković · D. Uskoković

Received: 18 October 2010 / Accepted: 12 January 2011 / Published online: 24 February 2011

Abstract In this study, the ZnO nanopowders were synthesized by mechanochemical processing with a successive thermal decomposition reaction. The initial reactants mixture of zinc chloride and oxalic acid was milled from 30 min to 4 h and thermally treated for 1 h at 450 °C. The influence of both, oxalic acid and the duration of milling, on the crystal structure, average crystallite size, average particle size, and the morphology of ZnO nanopowders were investigated. The qualitative analysis was performed using X-ray diffraction and Raman spectroscopy techniques. While the XRD analysis shows perfect long-range order and pure wurtzite structure of the synthesized ZnO powders, Raman spectroscopy indicates a different middle-range order; in addition, according to Raman spectra, it is found that lattice defects and impurities introduced in ZnO crystal structure depend on milling duration, in spite of applied thermal treatment. The particle size distribution was measured by laser diffraction, whereas the morphology of the powders was determined by scanning electron microscopy. Impurity contamination was studied using inductively coupled plasma analysis. The obtained results showed that the applied two-step method is appropriate for the synthesis of high crystalline ZnO nanopowders, with uniform spherical particles with diameter between 20 and 50 nm. Profound effect of aqueous solution of oxalic acid to prevent agglomeration of final product is presented.

A. Stanković · Lj. Veselinović · S. Marković · D. Uskoković (✉)
Institute of Technical Sciences of the Serbian Academy of Sciences and Arts, Belgrade, Serbia
e-mail: dragan.uskokovic@itn.sanu.ac.rs

S. D. Škapin
Jožef Stefan Institute, Ljubljana, Slovenia

Introduction

Zinc oxide, ZnO, is an attractive material because of its unique properties, such as optical transparency, electrical conductivity, piezoelectricity, and near-UV emission [1–6]. In particular, nanosized ZnO has wide application in (UV) lasers, solar cells, varistors, gas sensors, transparent UV resistance coatings, photo-printing, sunscreen lotions, cosmetics, and medical creams.

In recent years, many studies have been carried out to develop methods for the synthesis of ZnO nanoparticles. The morphology of ZnO nanoparticles strongly depends on the presence of different types of surfactants in the reaction system [7]. Commonly used methods to produce ZnO nanopowder are: precipitation [8], sol–gel process [9], ultrasound-assisted synthesis [10], hydrothermal/solvothermal synthesis [11], and mechanochemical processing [12]. Mechanical milling has been extensively used for the synthesis of nanocrystalline materials because of its simplicity, relatively low-cost equipment, the large scale production, and applicability for variety of materials. Ball-milling technique operates at room temperature, which increases safety and reduces energy utilization. In general, mechanochemical processing has been recognized as a powerful technique for the synthesis of a wide range of semiconducting nanomaterials [12, 13], magnetic materials [14], carbon nanotubes [15], etc., which could otherwise be difficult to prepare using conventional methods. It has been reported that mechanical milling induces not only morphological and structural changes of the particles but also modify their optical [11] and electrical [16] properties. Most of the investigated mechanochemical synthesis procedures were preformed using mixtures of the appropriate metal salt or hydrated metal salt and an inert matrix (process controlling agents, PCA), which function is to prevent

the agglomeration of the synthesized particles [17–24]. The mechanochemically assisted method involves mechanical activation of solid-state chemical reactions at low temperatures in a ball mill. This process is characterized by repeated welding and fracture of the reacting precursor particles through ball-powder collisions, which continually regenerate the reacting interfaces, allowing chemical reactions to occur. Milling reduces particle size, which results in an increase of the surface area available for reaction, leading to the formation of a nanosized intermediate compound. During the subsequent heat treatment separated nanocrystals surrounded by appropriate solid matrix of the desired phase were formed. Matrix phase usually can not be decomposed during the milling or thermal treatment, however, it can be simply removed by washing process in the final step [24].

There are three common reaction routes for the synthesis of ZnO nanoparticles by mechanochemical methods. The first is the milling a mixture of $ZnCO_3{\cdot}Zn(OH)_2$ and NaCl, as PCA, followed by the calcinations of the milled powder mixture [25]. This synthesis procedure has industrial application. The second one is a solid-state reaction of $ZnCl_2$ and Na_2CO_3 to form $ZnCO_3$ intermediate and NaCl as PCA by the subsequent thermal treatment of $ZnCO_3$ [19, 26], and the third is the milling of zinc acetate $Zn(CH_3COO)_2$ and oxalic acid $C_2H_2O_4{\cdot}2H_2O$ followed by a thermal decomposition reaction [27].

In our previous study [28] the influence of both, the milling time and the presence of an inert inorganic salt matrix, on the characteristics of ZnO and ZrO_2 powders have been investigated. The materials used for the preparation of the ZnO powder were $ZnCl_2$ and $Ca(OH)_2$. The mixture of the powders was treated in agate vials with alumina balls. The synthesized ZnO powder was consisted of nanoparticles, however, with wide particle size distribution (PSD) between 50 and 200 nm.

In this article, we extended our previous study to investigate Mechanical–Thermal Synthesis (MTS)—mechanical activation followed by thermal activation [29] of ZnO from $ZnCl_2$ and oxalic acid ($C_2H_2O_4{\cdot}2H_2O$) as reactants with the intention to obtain pure ZnO nanopowder. Furthermore, the aim of the study was to examine the effects of the oxalic acid as an organic PCA, and different milling times, on the crystal structure, average particle size, and the morphology of ZnO nanopowders.

Experimental procedure

The mixture of $ZnCl_2$ and $H_2C_2O_4{\cdot}2H_2O$ powders with a molar ratio of $2[HC_2O_4]^-:Zn^{2+}$ and total quantity of 19.4 g was sealed in an agate vial (500 mL) with alumina balls (Ø 8 mm). Milling was performed in a planetary ball mill Retsch PM4, using the ball-to-powder mass ratio 10:1. The mechanochemical processing was carried out for 30, 60, 120, and 240 min, at 180 rpm, applying reversal mode of milling. It can be emphasized that during the milling the increase in the vial temperature was not observed. In all examined cases, throughout the process of milling, reactants mixture was transformed in a paste state intermediere phase. The obtained pastes were dried at 100 °C for 1 h, yielding highly hygroscopic zinc oxalate powders. In the next step, as-prepared powders were thermally treated at 450 °C in air for 1 h. The temperature of 450 °C was chosen as the necessary for decomposition reaction from $ZnC_2O_4{\cdot}2H_2O$ to ZnO [20]. Every synthesis procedure was repeated at least twice. Synthesized ZnO powders were denoted as ZnO-30 to ZnO-240 according to milling time.

Furthermore, the influence of the wet-milling conditions on the ZnO average particle size and morphology is examined. For that purpose, instead the solid-phase oxalic acid as the initial reactant an aqueous solution of oxalic acid was used (12.6 g of oxalic acid in 25 mL of deionized water). As a result of water addition to the initial reactants mixture ball-to-powder mass ratio was changed to 4.4:1. All the other experimental conditions were equal to previous ones.

The list of prepared samples and experimental conditions is shown in Table 1.

The phase composition and average crystallite size of the prepared powders were investigated at room temperature using X-ray diffraction measurements. The XRD data were collected on a Philips PW-1050 automatic diffractometer with Cu $K_{\alpha 1,2}$ radiation, at 40 kV and 20 mA. The diffraction measurements were done over scattering angle 2θ from 0 to 80° using a step size of 0.02° and a counting time of 2 s per step. The Raman spectra of the powders were obtained as a result of the backscattering geometry using a μ-Raman system with a Jobin Yvon T64000 triple monochromator, equipped with a liquid nitrogen cooled charge-coupled-device (CCD) detector. The 514.5 nm line of an Ar-ion laser was used as an excitation source. The measurements were performed at a laser power of 80 mW. The Raman spectra were recorded in the frequency interval 50–1600 cm^{-1}. The morphology of the prepared ZnO powders was analyzed using a JEOL JSM-6460 LV scanning electron microscope (SEM) and field emission SEM (FE SEM) SUPRA 35 VP Carl Zeiss. The ZnO powders were gold-coated for SEM imaging, while for the FE SEM analysis the powders were dispersed in ethanol, filtrated, and then carbon coated.

The average particle size, PSD, and the nature of agglomerates were determined by the particle size analyzer (PSA) Mastersizer 2000 (Malvern Instruments Ltd., UK), based on laser diffraction, which covers the particle size range of 0.02–2000 μm.

The degree of contamination of the ZnO powders during mechanical treatment was determined using an inductively

Table 1 List of the prepared samples, experimental conditions, and calculated crystallite sizes

Samples	Reactants	Precursor	First-step milling time (min)	Second-step thermal decomposition	Crystallite size (nm)		
					[002]	[100]	[101]
ZnO-30	$ZnCl_2$ and $H_2C_2O_4{\cdot}2H_2O$	$ZnC_2O_4{\cdot}2H_2O$	30	450 °C, 1 h	41	46	40
ZnO-60			60		47	51	45
ZnO-120			120		35	38	34
ZnO-240			240		40	43	38
*ZnO-240			240		40	43	38

*ZnO-240 was synthesized in aqueous solution phase

coupled plasma spectrometer (iCAP Thermo Scientific 6300). The samples for analysis were diluted in concentrated HCl. Potential impurities can be introduced into the system due to physical or chemical interaction between the material of the container and/or milling medium with the reactants' mixture. In the experiments presented in this study, two chemical elements could appear as impurities, Al—from the alumina balls, and Si—from the agate vial.

Results and discussion

In the first-step of ZnO nanopowders synthesis, the mixture of reactants was milled from 30 min to 4 h. According to XRD pattern (Fig. 1a) after 30 min of mechanical milling, the diffraction peaks related to the $ZnCl_2$ completely disappeared, small amount of oxalic acid exists (sufficiency of oxalic acid is prearranged to work as PCA); furthermore, it is found that zinc oxalate $ZnC_2O_4{\cdot}2H_2O$ was produced. This indicates that energy developed during mechanical milling induced chemical reaction between the starting powders. Prolonged milling to 4 h did not change reaction product which implied second-step of synthesis—thermal decomposing of intermediere. XRD patterns of ZnO powders prepared by this two-step processing are presented in Fig. 1b–f. All of the reflections presented at the XRD patterns correspond to the single-phased ZnO with a wurtzite hexagonal structure (JCPDS Card No. 36-1451) [22]. The narrow reflections and low level of background confirm good crystallinity of the prepared ZnO powders.

Thus, according to X-ray data, two-step synthesis of ZnO nanopowder can be presented by following: the high-energy mechanical milling initiates mechanochemical reaction(s) between the starting powders, which leads to the formation of the zinc oxalate intermediere. The formation of zinc oxalate is described by the chemical reaction (1):

$$ZnCl_2 + C_2H_2O_4 \cdot 2H_2O \rightarrow ZnC_2O_4 \cdot 2H_2O + 2HCl. \quad (1)$$

In the second step, the zinc oxalate intermediere was thermally decomposed at 450 °C in air atmosphere [20] according to the chemical reaction (2),

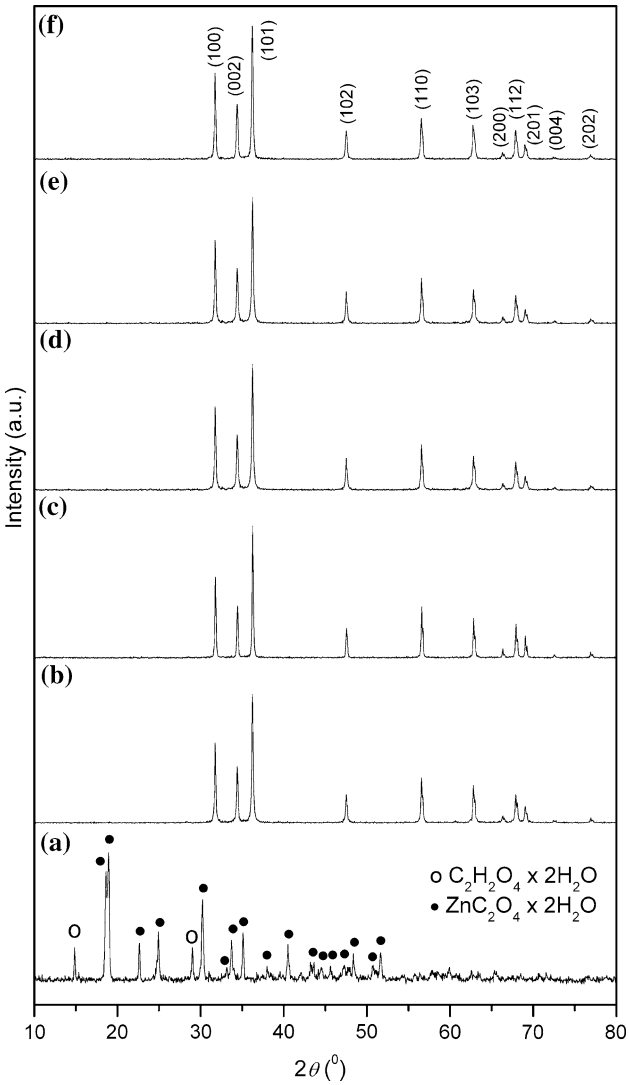

Fig. 1 XRD patterns of: (*a*) reactant precursors obtained after milling for 30 min; (*b*) ZnO-30; (*c*) ZnO-60; (*d*) ZnO-120; (*e*) ZnO-240, and (*f*) *ZnO-240

$$ZnC_2O_4 \cdot 2H_2O + 0.5O_2 \rightarrow ZnO + 2CO_2 + 2H_2O \quad (2)$$

yields to light yellow powder of ZnO [27, 30, 31].

Furthermore, the XRD data were used for the calculation of the ZnO crystallite size. The crystallites size (D) was calculated according to the Scherrer's equation (3):

$$D = \frac{K\lambda}{\beta_m \cos\theta}, \quad (3)$$

where λ is the wavelength of X-ray radiation; K is the shape coefficient and is approximately equal to one; θ is the diffraction angle (°) and β_m is the full width at half maximum of reflection at the diffraction angle (*radian*) [32, 33].

For calculation of crystallites size, three crystallographic directions [002], [100], [101], characteristic for hexagonal symmetry of ZnO, were chosen, allowing also estimation of their morphology. The obtained results refer to isometrically shaped crystallites of ZnO nanopowders. Moreover, crystallites sizes slightly depend on milling time. The calculated crystallites sizes are listed in Table 1.

So, the XRD pattern confirms the pure wurtzite structure of ZnO regardless of the mechanical milling duration. It is known from literature that prolonged mechanical milling can cause some crystalline defects in the crystal structure of ZnO. However, the existence of the single wurtzite phase in XRD patterns does not mean that the crystalline structure of ZnO has not been distorted by mechanical milling, since the crystalline defect may be of small size and not detectable by XRD. Otherwise, Raman spectroscopy is frequently used to study changes of the crystal structure, lattice defects, particle size, or introduction of secondary phases in ZnO materials since the Raman scattering signal is dependent on the electron–phonon interaction. Raman studies of ZnO materials have revealed a strong dependence of the spectral features on the nature and concentration of impurities present in the ZnO host lattice.

Hence, the effect of mechanical milling on the crystal structure of ZnO was studied by Raman spectroscopy. Hexagonal ZnO crystals with a wurtzite structure belong to the C_{6v}^4 ($P6_3mc$) space group with two formula units per primitive cell, where all atoms occupy 2b sites of C_{3v} symmetry. According to the group theory, the following optical modes are present: $\Gamma_{opt} = A_1 + 2B_1 + E_1 + 2E_2$. Among them, A_1, E_1, and E_2 are Raman active, whereas B_1 is forbidden. A_1 and E_1 are polar and split into transverse optical (A_1 TO and E_1 TO) and longitudinal optical (A_1 LO and E_1 LO). E_2 mode consists of two modes of low and high frequency phonons (E_2^{low} and E_2^{high}), which are associated with the vibration of the heavy ZnO sublattice and oxygen atoms, respectively. The room temperature Raman spectra of the prepared ZnO powders are shown in Fig. 2.

First of all, the Raman spectra of the investigated ZnO powders showed very high luminescence, indicating the particle size above the critical limit, i.e., the existence of nanoparticles with large surface-to-volume ratio. All modes that appear in the Raman spectra of the ZnO-30 (Fig. 2a) can be assigned to wurtzite structure [34]. The most intensive band is E_2^{low} at 99 cm^{-1}, attributed to vibrations of the zinc sublattice in ZnO [34, 35]. The peak at 335 cm^{-1} is assigned as the second-order acoustic mode. The sharp and strong peak at 438 cm^{-1} corresponds to the E_2^{high} mode of ZnO, and is assigned to oxygen vibration. The optical phonon peak at 542 cm^{-1} is assigned to the LO mode of A_1 symmetry. This broad band consists of two more bands, at 571 and 584 cm^{-1} which can be assigned to A_1 (LO) and E_1 (LO) modes, respectively. The appearance of the A_1 (LO) and E_1 (LO) bands in a Raman spectrum of ZnO is due to the formation of structural defects (oxygen vacancies and zinc interstitials), besides, the E_1 (LO) mode is more strongly affected by these effects [34]. The Raman peak located about 1120 cm^{-1} corresponds to the optical

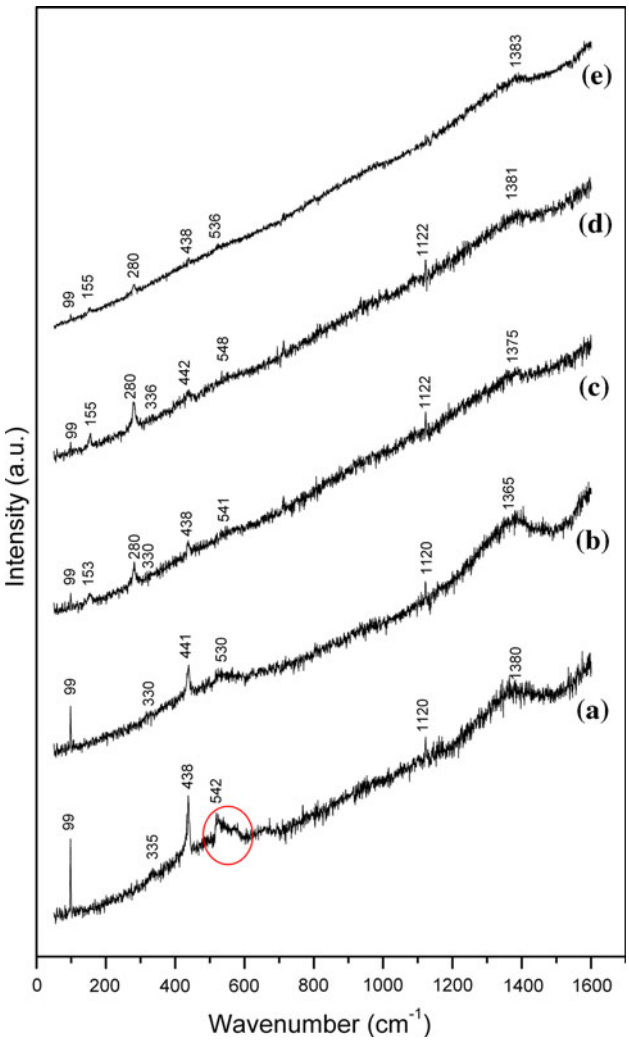

Fig. 2 Raman spectra of: (*a*) ZnO-30; (*b*) ZnO-60; (*c*) ZnO-120; (*d*) ZnO-240, and (*e*) *ZnO-240

overtone [36]. The peak at $\sim 1380\ cm^{-1}$ indicates three-phonon Raman scattering processes, A_1 (TO) + A_1 (LO) + E_2^{high} [37]. Thus, ZnO-30 has wurtzite hexagonal structure with introduced lattice defects. For the further analysis of the influence of the milling time on wurtzite structure three characteristic Raman bands were chosen: E_2^{low}, $E_2^{high}$and A_1 (LO) + E_1 (LO). Raman spectra of the ZnO-60 to *ZnO-240 powders, Fig. 2b–e, have E_2^{low} and E_2^{high} bands, which indicate the wurtzite crystal structure, and is in accordance with the results of XRD measurements. Furthermore, it is observed that the increases of milling time in first-step of synthesis process suppressed broad band in Raman spectra at 540–580 cm^{-1} attributed to A_1 (LO) + E_1 (LO) mode caused by defects. According to Raman spectra structural defects disappear after 2 h of milling yielding to ZnO powders of very good crystal quality. These results can be explained by ordering of precursor ZnC_2O_4 crystal structure during prolonged milling, which is further repercuted on crystal structure of ZnO. Furthermore, *ZnO-240 powder possesses the most ordered wurtzite crystal structure the (Fig. 2e) [38]. However, bands at near 155 and 280 cm^{-1}, which are not observed in spectra of ZnO-30 and -60, appear in the spectra of ZnO-120 to *ZnO-240. These bands are not characteristic for the wurtzite crystal structure; they represent second phase(s) and can be attributed to impurities introduced during milling.

Thus, although the XRD analysis shows a perfect long-range order, i.e., a pure wurtzite crystal structure for all of the ZnO powders, Raman spectroscopy indicates that at the middle-range scale, lattice defects and impurities introduced into ZnO powders depend on milling time, in particular, prolonged milling reduces crystal defects but introduces impurities.

Effect of milling time onto morphology of final ZnO powders was examined by SEM, Fig. 3. According to the SEM image of the ZnO-30, Fig. 3a, b, it can be seen that the most of the particles are organized in agglomerates with dimensions up to a 1 μm. Figure 3c, d represent morphology of ZnO-60; it can be noticed that prolonged milling time up to 1 h yields small changes in the particles morphology. There are no clearly separated particles; agglomeration is still obvious. In the samples ZnO-120, Fig. 3e, f, and ZnO-240, Fig. 3g, h, important changes in particle shape are obvious. From Fig. 3f, h it is evident that a prolonged mechanochemical process yields almost geometrically ideal spheres of ZnO. There are lots of isolated single particles, hence agglomeration is not dominant. A significant reduction in the particle size is achieved: the sample milled for 2 h had particles with an average diameter between 120 and 140 nm (Fig. 3f), while after 4 h of milling the average diameter decreased to between 50 and 90 nm (Fig. 3h). These data collected from the SEM micrographs indicate that the morphology of the ZnO particles as well as their consistence (agglomeration) are determined by the duration of the milling process, regardless to the applied thermal treatment. Precisely, prolonged milling reduced particle size, improved their geometrical shape and softened agglomerates. This can be explained by following: milling of $ZnCl_2$ and $H_2C_2O_4 \cdot 2H_2O$ led to the formation of nanocrystalline zinc-oxalate precursor which was partly isolated in the organic matrix. This prevented the agglomeration of the particles during the thermal treatment since organic matrix can not be thermally decomposed.

Hence, the particle size estimated from the SEM images is ranged between 50 and 140 nm. Furthermore, the PSD was measured by a laser PSA and results are represented over number and volume. Since the synthesized powders are mostly the agglomerates of the primary nanoparticles, the correctness of this measurement technique depends on the quality of the powder dispersion. Here, after the powders were dispersed for 30 s with the aid of low-intensity ultrasound, the following results were obtained: the number-based PSD was very narrow; 10% of particles (d_{10}) were smaller than 35 nm, 50% of particles (d_{50}) were approximately 60 nm in size, while more than 90% (d_{90}) of the particles were smaller than 130 nm. The results presented over volume are noticeably different; in particular, particles are agglomerates with d_{90} between 18 and 27 μm, depending on milling time. Precisely, for the sample milled 30 min d_{90} is 21 μm, after 1 h of milling d_{90} increased up to 22.5 μm, while prolonged milling time of 2 h yield agglomerates with dimensions of 27 μm. Finally, after 4 h of milling a reduction of agglomerates is observed i.e., d_{90} decreases to 18 μm. The corresponding PSDs over number and volume, with the inserted values of d_{10}, d_{50}, and d_{90} are presented at right-hand side of Fig. 3. This is valid for all ZnO powders whose morphology is presented in Fig. 3. It can be emphasized that the synthesized ZnO powders are uniform nanopowders.

According to the results of number-based PSD, where during 30 s of low-intensity irradiation of the ZnO powders the existing agglomerates (up to 1 μm) were fractured into primary particles (down to 50 nm), it can be concluded that during low-temperature calcination soft aggregates were formed with weak van der Waals forces between particles, without a sintering process. A large discrepancy between d_{10}, d_{50}, and d_{90} presented over number and volume can be explained by existence of a large number of isolated ZnO nanoparticles occupying a small volume in measurement batch during PSA simultaneously with a neglected number of voluminous agglomerates conserved during ultrasound dispersion.

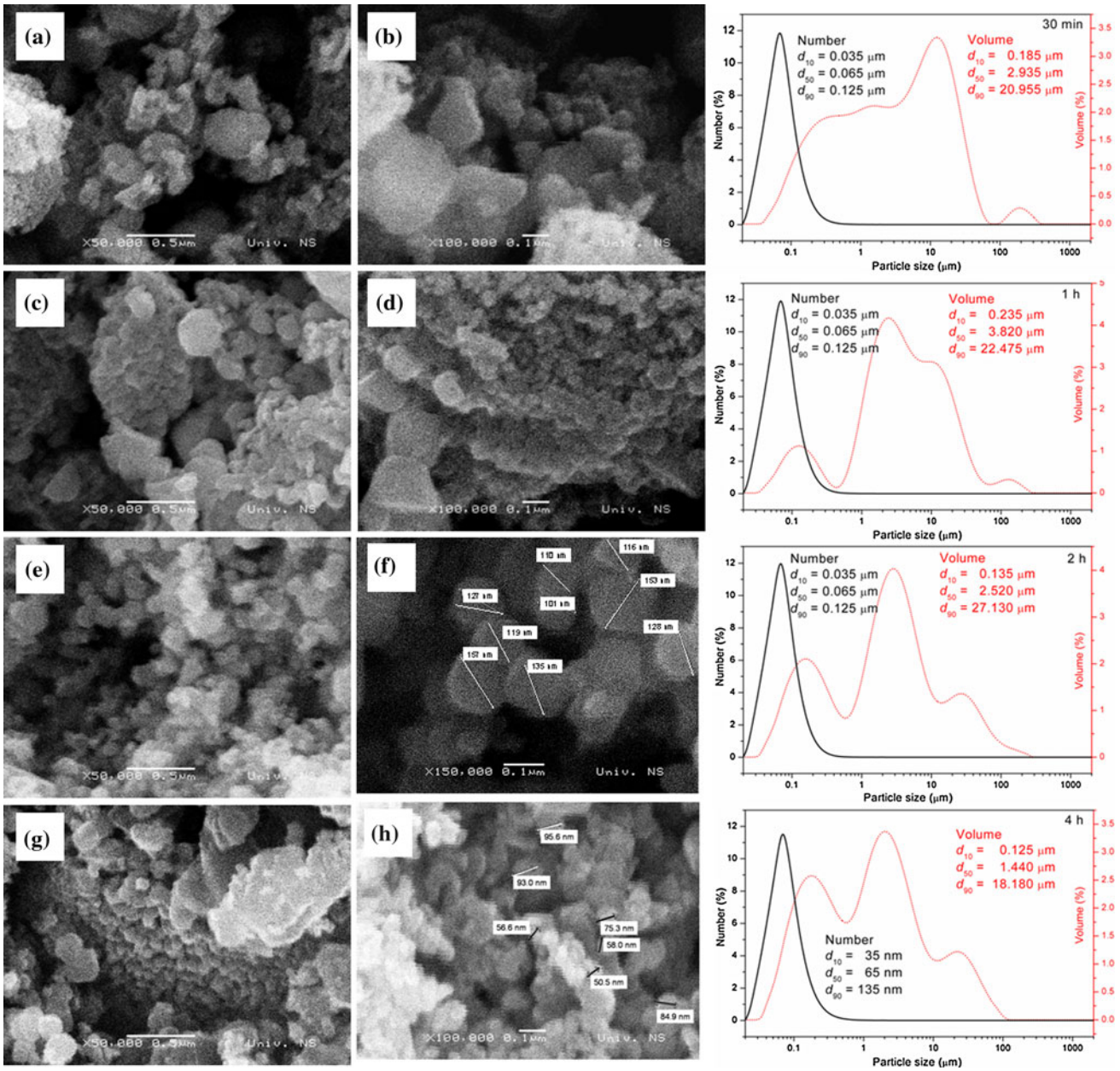

Fig. 3 SEM images of: **a**, **b** ZnO-30; **c**, **d** ZnO-60; **e**, **f** ZnO-120, and **g**, **h** ZnO-240. Low-magnification images (×50,000): (**a**), (**c**), (**e**), and (**g**); high-magnification images (×100,000): (**b**), (**d**), (**f**), and (**h**). Corresponding PSDs are presented on the *right side*

The number-based average particle size of a ZnO nanocrystal, around 60 nm, as observed from the particle size analysis and the SEM data, well matched with the crystallite size calculated from the line shape of X-ray diffraction.

Some improving results were obtained from SEM of the *ZnO-240. The size of the synthesized ZnO particles was comparable to that of the particles in the sample milled without the presence of water, but with increased diameter uniformity. Furthermore, the milling in the aqueous solution of oxalic acid decreased the agglomeration of the formed ZnO particles. The corresponding SEM images are given in Fig. 4: in (a) low magnification (×50,000) and in (b) high (×150,000) magnification. The ZnO particles show almost ideal spherical shapes, they are well dispersed and non-agglomerated, with a diameter ranging between 15 and 50 nm, Fig. 4a–d. The PSD over number and volume, with the inserted values of d_{10}, d_{50}, and d_{90} is presented at the bottom of Fig. 4. Number-based PSD is very similar to the above presented (Fig. 3). Furthermore, volume-based PSD confirms the presence of softer agglomerates of the ZnO nanoparticles. Precisely, a larger reduction of

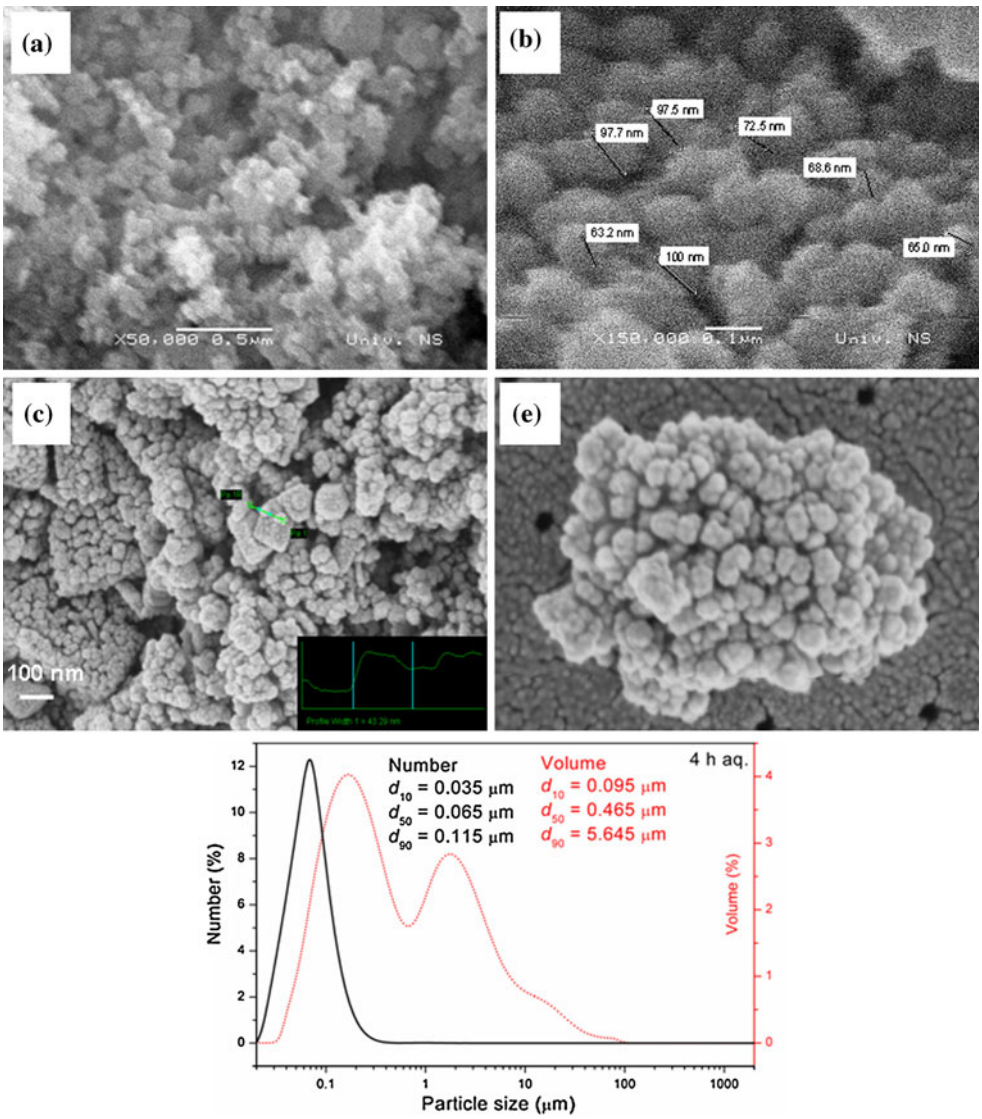

Fig. 4 SEM (**a**, **b**) and FE SEM (**c**, **d**) images and (*bottom*) corresponding particles size distributions of *ZnO-240

agglomerates diameter ($d_{90} \sim 5.6$ µm) is observed for the sample milled for 4 h in the presence of aqueous solution of oxalic acid compared to the result for the sample milled without the presence of water ($d_{90} \sim 18$ µm) for the same milling time. These results indicate that the wet-milling conditions are favorable for production of ZnO nanosized powders with small number of soft agglomerates.

The number-based particle dimensions observed by a laser PSA (35–115 nm) are somewhat larger than the corresponding dimensions estimated from the SEM micrographs (15–50 nm). The discrepancy is probably due to the tendency of the active ZnO primary particles to aggregates in water dispersion during the measurements of the size distribution. Hence, in spite of true particle size, the results of PSA indicate the size of ZnO aggregates.

Here we want to explain an improving effect of milling in aqueous solution of oxalic acid compared to dry milling in solid oxalic acid. In the both cases oxalic acid has twofold function; it acts as the reactant involved in synthesis procedure, and as PCA [21, 39]. During the dry milling process, zinc-oxalate precursor was partly isolated in the small sufficiency of organic matrix, which prevents the agglomeration of the ZnO particles during the thermal decomposition of zinc oxalate. On the other hand, the aqueous solution of oxalic acid decreases viscosity of the slurries, the PCA coated a large surface area of the precursor particles [40, 41]. It results in less disorderly fluted and smoother surfaces, which improves the applicability of the resulting products made from the ceramic powder. As a result of an appropriate pH range in the starting reactant mixture, oxalic acid plays another very important role in the synthesis process. As a passivating agent, it ensures a relatively uniform surface charge on the ceramic particles, providing an electrostatic barrier to agglomeration. Hence, the profound effect of oxalic acid as the starting reactant and the passivating agent was shown. In addition, it is

Table 2 Concentrations of Si and Al in the ZnO powders

Samples	Concentration (μg/g)	
	Si	Al
ZnO-30	/	/
ZnO-60	/	/
ZnO-120	285	380
ZnO-240	400	525
*ZnO-240	940	575

shown that by design of oxalic acid viscosity the degree of agglomeration can be controlled.

Since Raman spectroscopy indicates existence of second phase in the ZnO powders, inductively coupled plasma (ICP) emission spectroscopy was used to determine the degree of contamination of the powders during the mechanical treatment. Two elements can be considered as possible impurities, Al from the alumina balls and Si from the agate vial. The concentrations of the impurities are listed in Table 2; the amount of foreign elements increases with the increasing of milling time, which is typically for mechanochemistry. The *ZnO-240 powder contains the highest amount of impurities, especially Si; that can be explained by lower viscosity of aqueous solution of oxalic acid (PCA) which allowed stronger collisions between the balls and the agate vial. However, the highest amount of second phases is less than 2% wt.

Conclusions

In this article, the results of a detailed study of a controlled mechanochemically assisted synthesis of ZnO nanopowders in the presence of oxalic acid were presented. The mixture of initial reactants (zinc chloride and oxalic acid), was milled from 30 min up to 4 h, and subsequently annealed at 450 °C for 1 h. The influence of both oxalic acid and the duration of milling on the properties on the final ZnO powders were investigated. The qualitative analysis of the prepared powders was performed using XRD and Raman spectroscopy. The XRD analysis showed perfect long-range order and pure wurtzite structure of the synthesized ZnO powders, irrespective of the milling duration. Quite contrary, Raman spectroscopy indicates a different middle-range order of the ZnO powders. According to the Raman spectra it can be concluded that lattice defects and impurities introduced in the ZnO crystal structure depend on the milling duration; precisely, prolonged milling improved ZnO crystal structure by reducing of crystal defects, but introduced impurities. Moreover, room-temperature Raman spectra of ZnO nanopowders showed high luminescence.

From the SEM images, it is observed that the morphology of the particles strongly depends on the milling time of the reactants mixture, regardless of the further thermal treatment. The sample milled for 30 min contained particles organized in agglomerates with dimensions of a micron. Prolonged milling yielded almost geometrically perfect spheres of ZnO as well as a significant reduction in the average particle size; after 4 h of milling the average diameter decreased to 50 and 90 nm. The number-based average particle size of the ZnO powders estimated by the dynamic light scattering and SEM analyses was approximately 60 nm, which is well matched with the average crystallite size calculated from the line shape of X-ray diffraction (from 40 to 50 nm).

Moreover, this study demonstrated the profound effect of aqueous solution of oxalic acid as the starting reactant and the passivating agent in the first-step of ZnO synthesis. While ZnO powders with average particles between 50 and 90 nm were prepared using a dry milling process, during the wet-milling procedure the average particle size is reduced to between 15 and 50 nm. Evidently, separable crystalline ZnO particles with no significant agglomeration were obtained. In addition, the synthesized ZnO particles were almost ideal spheres. Hence, it is shown that by design of oxalic acid viscosity the degree of agglomeration can be controlled. This synthesis method may potentially be used for the commercial production of fine ZnO powders.

Acknowledgements The authors would like to thank Dr. M. Bokorov for SEM and Dr. B. Hadzić for Raman spectroscopy examinations. This study was supported by The Ministry of Science and Technological Development of the Republic of Serbia under grant no. III45004.

References

1. Look DC (2001) Mater Sci Eng B 80:383
2. He R, Choi H (2002) Adv Funct Mater 12:323
3. Huang MH, Mao S, Feick H, Yan H, Wu Y, Kind H, Weber E, Russo R, Yang P (2001) Science 292:1897
4. Shiono T, Yamamoto H, Nishino S (2004) Jpn J Appl Phys 43:4941
5. Sato T, Tanigaki T, Suzuki H, Saito Y, Kido O, Kimura Y, Kaito C, Takeda A, Kaneko S (2003) J Cryst Growth 255:313
6. Hochepied JF, Almeida de Pliveira AP (2004) Prog Colloid Polym Sci 125:68
7. Usui H (2009) Mater Lett 63:1489
8. Demir MM, Munoz-Espi R, Lieberwirth I, Wagner G (2006) J Mater Chem 16:2940
9. Tokumoto MS, Briois V, Samntilli CV (2003) J Sol-Gel Sci Technol 26:547
10. Bhatte KD, Fujita S, Arai M, Pandit AB, Bhanage BM (2011) Ultrason Sonochem 18:54
11. Zhang J, Sun L, Yin J, Su H, Liao C, Yan C (2002) Chem Mater 14:4172
12. Senna M, Nakayama S (2009) J Alloys Comp 483:265

13. Glushenkov AM, Zhang HZ, Zou J, Lu GQ, Chen Y (2007) Nanotechnology 18:175604
14. Shen TD, Schwarz RB, Tompson JD (2005) Phys Rev B 72:014431
15. Chen Y, Conway MJ, Fitzgerald JD (2003) Appl Phys A 76:633
16. Kuga Y, Shirahige M, Fujimoto T, Ohira Y, Ueda A (2004) Carbon 42:293
17. Fah CP, Xue J, Wang J (2002) J Am Ceram Soc 85:273
18. Baranov AN, Panin GN, Kang TW, Oh Y (2005) Nanotechnology 16:1918
19. Tsuzuki T, McCormick PG (2001) Scr Mater 44:1731
20. Kanade KG, Kale BB, Aiyer RC, Das BK (2006) Mater Res Bull 41:590
21. Adair JH, Shrout TR, Messing GL, Pecora TM, Mandanas MM (2002) WO Patent 0230572
22. Li YX, Chen WF, Zhou XZ, Gu ZY, Chen CM (2005) Mater Lett 59:48
23. Ding J, Tsuzuki T, McCormick PG (1996) J Am Ceram Soc 79:2956
24. Tsuzuki T, McCormick PG (1997) Appl Phys A 65:607
25. McCormick PG, Tsuzuki T (2003) US Patent 006503475
26. Aghababazadeh R, Mazinini B, Mirhabibi A, Tamizifar M (2006) J Phys Conf Ser 26:312
27. Shen L, Bao N, Yanagisawa K (2003) Chem Lett 32:826
28. Čeliković A, Kandić Lj, Zdujić M, Uskoković D (2007) Mater Sci Forum 555:279
29. Reddy BSB, Das K, Das S (2007) J Mater Sci 42:9366. doi: 10.1007/s10853-007-1827-z
30. Shen L, Bao N, Yanagisawa K, Domen K, Guptal A, Grimes CA (2006) Nanotechnology 17:5117
31. Małecka B, Drożdż-Cieśla E, Małecki A (2004) Thermochim Acta 423:13
32. Klug HP, Alexander LE (1954) X-ray diffraction procedures for polycrystalline and amorphous materials, 1st edn. Wiley, New York
33. Pardeshi SK, Patil AB (2009) J Mol Catal A Chem 308:32
34. Cuscó R, Alarcón-Lladó E, Ibáñez J, Artús L, Jiménez J, Wang B, Callahan MJ (2007) Phys Rev B 75:165202
35. Lin KF, Cheng HM, Hsu HC, Hsieh WF (2006) Appl Phys Lett 88:263117
36. Kaschner A, Haboeck U, Strassburg M, Strassburg M, Kaczmarczyk G, Hoffmann A, Thomsen C (2002) Appl Phys Lett 80:1909
37. Zhao J, Yan X, Yang Y, Huang Y, Zhang Y (2010) Mater Lett 64: 569
38. Giri PK, Bhattacharyya S, Singh DK, Kesavamoorthy R, Panigrahi BK, Nair KM (2007) J Appl Phys 102:093515
39. Wahab R, Ansari SG, Kim YS, Seo HK, Kim GS, Khang G, Shin HS (2007) Mater Res Bull 42:1640
40. Avvakumov E, Senna M, Kosova N (2002) Soft mechanochemical synthesis. Kulwer Academic Publishers, New York
41. Adair JH, Constantino AS (2003) US Patent 006514894